

Dual-Functional Implants with Antibacterial and Osteointegration-Promoting Performances

Yujie Sun,^{†,§} Yu-Qing Zhao,^{‡,§} Qiang Zeng,[†] Yu-Wei Wu,[†] Yang Hu,[‡] Shun Duan,^{*,‡} Zhihui Tang,^{*,†} and Fu-Jian Xu^{*,‡}

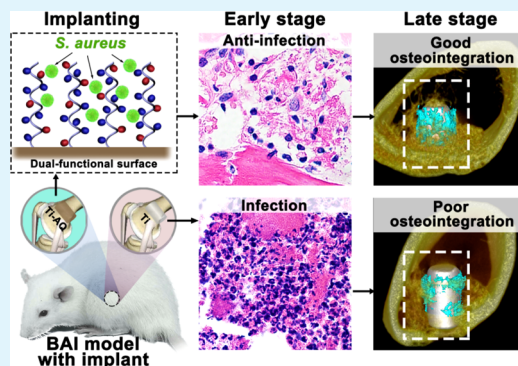
[†]Second Clinical Division, National Clinical Research Center for Oral Diseases, National Engineering Laboratory for Digital and Material Technology of Stomatology, Beijing Key Laboratory of Digital Stomatology, Peking University School and Hospital of Stomatology, Beijing 100101, China

[‡]Key Lab of Biomedical Materials of Natural Macromolecules, Ministry of Education, Beijing Laboratory of Biomedical Materials, Beijing Advanced Innovation Center for Soft Matter Science and Engineering, Beijing University of Chemical Technology, Beijing 100029, China

Supporting Information

ABSTRACT: Multifunctional antibacterial materials have great significance for treating biomedical device-associated infections (BAIs). In the present work, a facile and rational strategy was developed to produce dual-functional implants with antibacterial and osteointegration-promoting properties for the treatment of BAI. A titanium implant, as a representative demo of implants, was first functionalized with ethanediamine-functionalized poly(glycidyl methacrylate) (PGED) brushes. Then, low-molecular-weight quaternized polyethyleneimine (QPEI, a cationic antibacterial agent) and alendronate (ALN, a clinically used drug with high affinity for bone minerals) were covalently conjugated onto PGED brushes to produce dual-functional dental implants (Ti-AQ). The QPEI component imparted Ti-AQ with antibacterial abilities, and the ALN component could balance the cytotoxicity of a cationic antibacterial agent, improving the biocompatibility for osteoblast cells. The effective performances of anti-infection and osteointegration were demonstrated in a BAI animal model. The results indicated that Ti-AQ inhibited bacterial infection at the early stage and enhanced the osteointegration and biomechanical properties between the implants and bone tissues at the late stage. This study will provide one facile and universal strategy for the design and development of novel multifunctional antibacterial implants.

KEYWORDS: implant, antibacterial, surface modification, multifunction, osteointegration



1. INTRODUCTION

For many decades, biomedical device-associated infection (BAI) caused by bacteria has resulted in great amounts of failures in implantation therapy.^{1–3} Severe BAI is a devastating complication, which will cause pain, loss of function, systemic illness, and even death.^{4,5} It is well known that dental implantation is a typical implant-dependent therapeutic method. Dental implants are widely manufactured by titanium due to its excellent physical, chemical, and biocompatible properties and resistance to corrosion.⁶ However, pristine titanium implants have no antimicrobial properties, while oral cavity is an opening environment with multiple bacteria. Due to the complex bacterial spectrum in the oral microenvironment, BAI in dental implantation occurs with high incidence, which will lead to peri-implantitis.^{7,8} Thus, antibacterial surface functionalization of implants is the key point to reduce the morbidities of BAI.^{9,10} Diverse strategies have been developed to construct implants with antibacterial surfaces,^{11–16} such as antibiotic loading,¹⁷ nanoscience-based technologies,¹⁸ electrophoretic deposition,¹⁹ layer-by-layer immobilization,²⁰ photo-

thermal coating,²¹ photosensitizer modification,²² and polymer brush functionalization.^{23–26} Among them, surface functionalization with polymer brushes has drawn greater attention due to the nonreleasing property, facile preparation, and potential for postmodification with biofunctional agents.

By covalent conjugation of polymer brushes on the surface of biomedical materials, efficient antibacterial properties could be achieved.^{27–32} However, the single-functional antibacterial materials do not fulfill the comprehensive requirements of ideal implants, such as biocompatibility and bioactivity. Therefore, multifunctional antibacterial materials are desirable.³³ Although many methods have been developed for antibacterial and osteogenesis-enhancing functionalization, such as peptide anchorage,³⁴ silver deposition,³⁵ and hydrogel coating,³⁶ facile and flexible strategies for construct dual-functional implants still remain challenging. Various bioactive molecules could be

Received: August 14, 2019

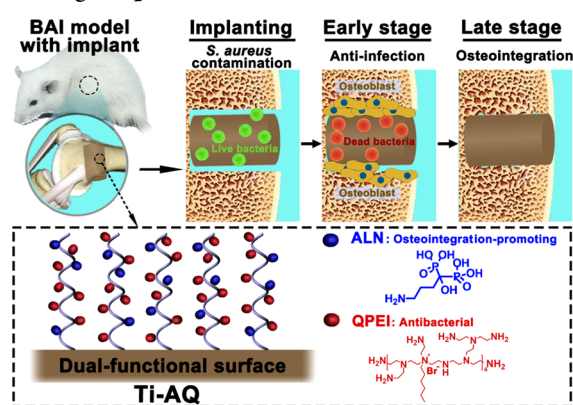
Accepted: September 18, 2019

Published: September 18, 2019

conjugated to polymer brushes with rich reactive groups.³⁷ By postmodification of polymer brushes, the surfaces of implants could possess versatile properties.^{38–40} In addition to antibacterial function, osteointegration-promoting property is also essential for dental implants, which will enhance the implant stability.¹³ For implantation therapy, it is critical to balance the antibacterial and osteointegration-promoting properties of implants.^{41,42} By flexible polymer brushes, it is promising to develop dual-functional implants with balanced antibacterial and osteointegration-promoting abilities.

In this work, dual-functional implants with antibacterial and osteointegration-promoting properties were constructed by using the postfunctionalization of polymer brushes (Scheme 1). The novelty of this work is the facile and flexible strategy

Scheme 1. Schematic Illustration of Dual-Functional Dental Implants with Antibacterial and Osteointegration-Promoting Properties



for constructing dual-functional surface by polymer brushes with plentiful reactive groups to conjugate bioactive molecules. Under mild conditions (room temperature and aqueous solution), various kinds of bioactive molecules with amino groups could be conjugated onto the polymer brushes with

high density. Moreover, the conjugated molecules are non-releasing due to the covalent linkage with the polymer brushes, which avoid the side effects induced by released components. Specifically, ethanediamine-functionalized poly(glycidyl methacrylate) (PGED) brushes with plentiful reactive groups were grafted from Ti implants via surface-initiated atom transfer radical polymerization (ATRP) (Figure S1, Supporting Information). Then, low-molecular-weight quaternized polyethyleneimine (QPEI, an efficient cationic antibacterial agent with plentiful amino groups) and alendronate (ALN, a typical diphosphonate with high affinity for bone minerals⁴³) were simultaneously conjugated by covalent bonds to the polymer brushes under mild conditions to construct nonreleasing dual-functionalized implants (Ti-AQ). The Ti-AQ implants were expected to possess high antibacterial efficiency against *Staphylococcus aureus* and good biocompatibility for osteoblast cells. The in vivo anti-infection and osteointegration-promoting performances of Ti-AQ were evaluated in a BAI animal model. The present work will provide useful information about the development of multifunctional implants to solve the clinical problems of BAI.

2. RESULTS AND DISCUSSION

2.1. Characterization of Dual-Functionalized Implants.

The detailed functionalization process of the dual-functionalized implant (Ti-AQ) with antibacterial and osteointegration-promoting properties is illustrated in Figure S1 (Supporting Information). First, a brown polydopamine layer was formed on Ti implants by self-polymerization of dopamine under alkaline conditions in the presence of oxygen, providing reactive sites (including hydroxyl and amino groups) for introducing initiators of ATRP.⁴⁴ Then, 2-bromoisobutyryl bromide was introduced onto the surface of Ti implants and poly(glycidyl methacrylate) (PGMA) brushes were grafted from the surface of implants via surface-initiated ATRP. Then, PGMA brushes were postmodified successively with ethanediamine by a ring-opening reaction and glutaraldehyde (GA) by a Schiff base reaction to produce functionalized Ti implants

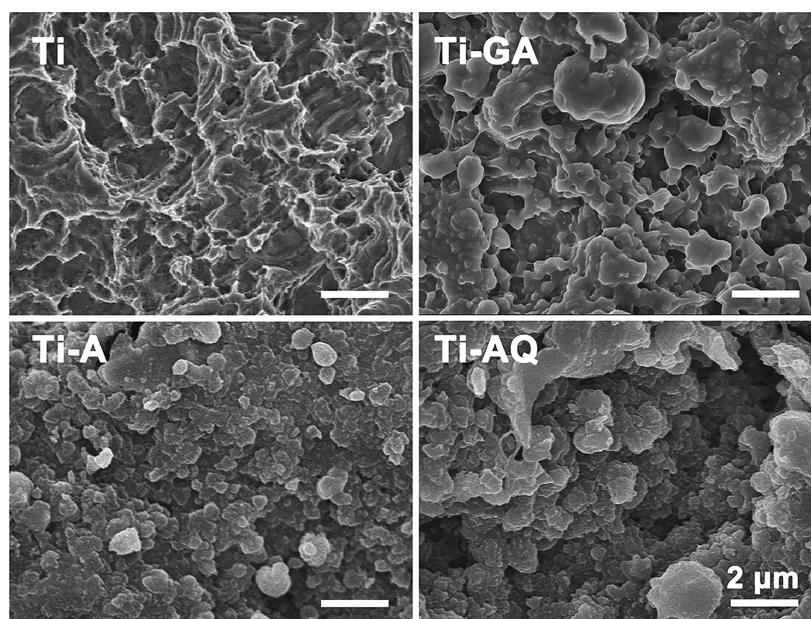


Figure 1. SEM images of Ti, Ti-A, Ti-Q, and Ti-AQ.

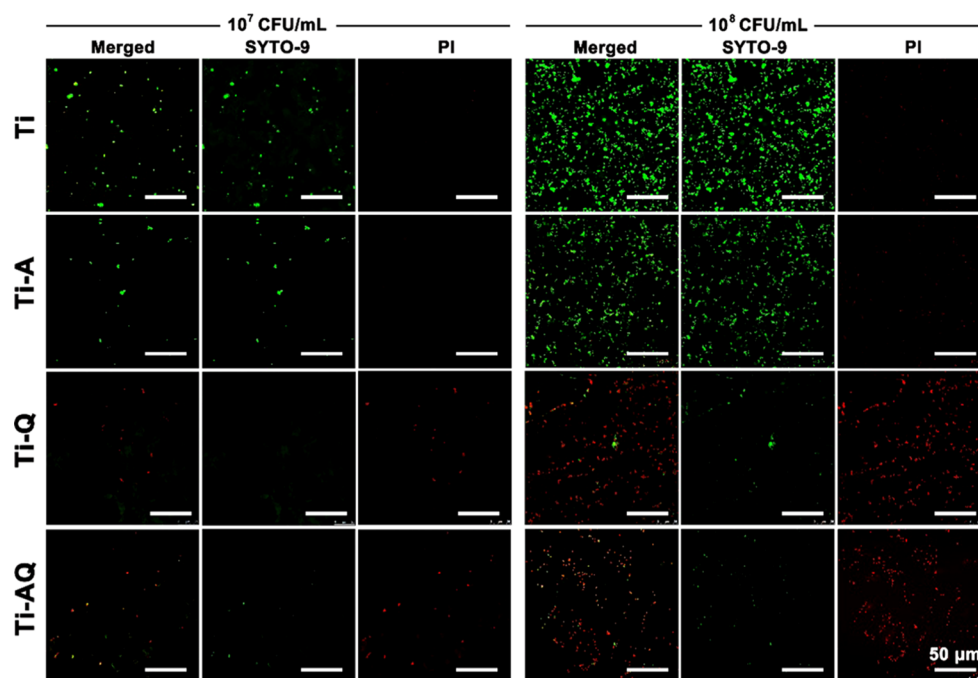


Figure 2. Representative CLSM images with different densities of *S. aureus* on Ti, Ti-A, Ti-Q, and Ti-AQ surfaces.

(Ti-GA) with abundant aldehyde groups. Finally, quaternized polyethyleneimine (QPEI with a quaternization degree of ~46%, an antibacterial component, Figure S2, Supporting Information) and alendronate (ALN, a bone-affinitive component) were covalently conjugated to Ti-GA by non-degradable C–N bonds and excessive QPEI and ALN were removed from the surface by rinsing thoroughly. Compared with other strategies, such as hydroxyapatite coating, alkali-heat treatment, acid etching, grit blasting, anodic oxidation, and growth factor grafting, this strategy was facile and flexible for multifunctionalization because of the plenty of reactive groups on polymer brushes. By this strategy, the Ti implant with antibacterial and osteointegration-promoting properties (Ti-AQ) was readily produced, while the Ti implants functionalized respectively with ALN (Ti-A) or QPEI (Ti-Q) were used as controls.

The functionalization process was confirmed by a scanning electron microscope (SEM), water contact angle (WCA), attenuated total reflection Fourier transform infrared (ATR-FTIR) spectroscopy, and X-ray photoelectron spectroscopy (XPS). Due to the pretreatment of sandblasting and acid etching, the Ti implants showed a highly rough topography (Figure 1a). Compared with being modified with polydopamine (PDA), the thickness of the polymer layer increased after functionalization with polymer brushes, which demonstrated that the polymer brushes were successfully grafted on the surface (Figure S3, Supporting Information). The WCA of Ti-GA was ~130° due to the hydrophobic aldehyde groups (Figure S4, Supporting Information). After being modified with ALN, QPEI, and ALN/QPEI, the WCAs of Ti-A, Ti-Q, and Ti-AQ decreased largely. On the surface of Ti-GA, the strong peak at the wavenumber of 1730 cm⁻¹ in ATR-FTIR spectra indicated the presence of C=O bonds of ester groups, while the characteristic peak of C=O bonds of Ti-Br was very weak, which demonstrated the successful grafting of polymer brushes (Figure S5, Supporting Information). Also, the N 1s signals at the binding energy of 399 eV of Ti-A, Ti-Q, and Ti-

AQ were attributed to the C–N bond in the reduced Schiff base structure, proving the successful postmodification of multialdehyde polymer brushes (Figure S6, Supporting Information). Moreover, the P 2p signals at the binding energy of 133 eV of Ti-A and Ti-AQ indicated that ALN had been conjugated to the polymer brushes. In the N 1s spectra of Ti-Q and Ti-AQ, the characteristic peak at the binding energy of 402 eV was ascribed to the strong electron-withdrawing environment of a quaternized ammonium group, revealing the existence of the QPEI component on the surfaces of Ti-Q and Ti-AQ (Figure S6, Supporting Information). Both QPEI and ALN have –NH₂ in the molecular structures; therefore, QPEI and ALN might compete with each other during the Schiff base reaction. The feeding molar ratio of QPEI/ALN was about 1:10. However, QPEI possesses much more amino groups (18 amino groups per molecule) than ALN (one amino group per molecule) and the steric hindrance of QPEI does not significantly affect the reaction due to the branched molecular structure. Based on the atom ratio of nitrogen and phosphorus (Table S1, Supporting Information), the [QPEI]/[ALN] molar ratio on the Ti-AQ surface was determined to be about 2/1. The above results demonstrated the successful preparation of Ti-A, Ti-Q, and Ti-AQ.

2.2. In Vitro Biological Performances of Ti-AQ. Among the complex bacterial spectrum in the oral microenvironment, the BAI in clinic of dentistry is mainly induced by *S. aureus*.^{7,8} In the present study, the antibacterial abilities of dual-functionalized implants were evaluated with *S. aureus* as a modal pathogen by confocal laser scanning microscope (CLSM) images of live/dead analysis, in which live bacteria were shown in green fluorescence and dead bacteria were in red (Figure 2). The pristine Ti implant had no antibacterial ability. At the low density of feed bacteria (10⁷ CFU mL⁻¹), Ti-AQ showed higher antibacterial efficiency of 93.8% than that of Ti-A because the cationic component QPEI could damage cell membranes by contact with bacteria and lead to cell death.⁴⁵ In addition, the amounts of bacteria adhering on

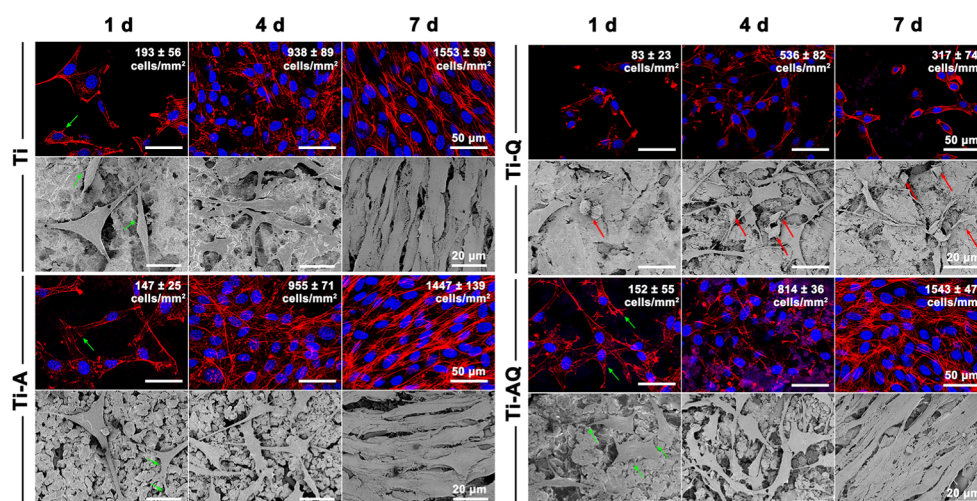


Figure 3. Representative CLSM and SEM images of MC3T3-E1 cells on the surfaces of Ti, Ti-A, Ti-Q, and Ti-AQ at 1–7 days. The numbers presented the cell density of each surface. Green arrows pointed the lamellipodia and filopodia of MC3T3-E1 cells.

the surfaces of Ti-A and Ti-AQ were lower than that on the Ti surface, indicating that the functionalized implants could reduce the adhesion of bacteria due to the plenty hydroxyl groups from the ring-opening reaction of PGMA,²⁶ which might lower the risks of infection under low amount of bacteria. When the density of feed bacteria became higher (10^8 CFU mL⁻¹), Ti-AQ still exhibited strong antibacterial activity, showing an antibacterial ratio of 95.6% (Figure 2). Because of the cationic component QPEI, the Ti-Q possessed strong bactericidal efficiency on 10^7 and 10^8 CFU mL⁻¹ of bacteria. The above results exhibited that Ti-AQ had effective antibacterial properties and was promising for the therapy of BAI in vivo.

For ideal medical implants, in addition to the antibacterial ability, the implant surface, especially the surface with cationic antibacterial agents, also should have good biocompatibility to support the growth and migration of mammalian cells. Thus, MC3T3-E1 osteoblast, a commonly used cell line for biocompatibility evaluation of bone-related materials, was seeded onto the surfaces of Ti, Ti-A, Ti-Q, and Ti-AQ. To evaluate the cytotoxicity of dual-functionalized implants, the adhesion, proliferation, and morphology of MC3T3-E1 on the surfaces of each group of samples were assessed by CLSM, SEM, and cell counting at 1–7 days (Figure 3). Initial cell adhesion is the first cellular event during cell–implant interactions, which is a critical factor that determines the clinical success of implants.⁴⁶ After 1 day culture, the osteoblast cells could adhere and spread as spindle or star cell shapes on the surfaces of implants. Moreover, visible microfilaments, lamellipodia, and filopodia in different directions were observed (green arrows in Figure 3), indicating that the cells were live and firmly anchored on the surfaces. On the contrary, round cells were present on the Ti-Q surface, indicating that the cells did not adhere well on the surface (red arrows in Figure 3).

The cells grew continuously with culture time, showing similar cell morphologies in all of the three groups. At day 4, the osteoblast cells proliferated and bridged with adjacent cells into a network on the surfaces of Ti, Ti-A, and Ti-AQ, while the proliferation rate of cells on Ti-Q was slower. After 7 day culture, the cells grew into multiply layers and presented as directional sheets. In contrast, the cell density on Ti-Q

decreased. In addition, the cell densities on each surfaces were quantified (inserted numbers in Figure 3). The results of quantitative analysis showed that no significant differences were observed among the cell densities on the Ti, Ti-A, and Ti-AQ surfaces. However, Ti-Q showed significant cytotoxicity, which led to obvious cell death (red arrows in Figure 3). These results suggested that the process of dual functionalization had no adverse effects on the adhesion, proliferation, and morphologies of osteoblast cells, indicating the good biocompatibility of Ti-AQ. When the cationic antibacterial components were applied alone, they could affect biocompatibility by causing toxicity to mammalian cells.^{47,48} It was reported that the introduction of suitable negatively charged groups into the molecular structure of antibacterial polymers could reduce cytotoxicity with little influence on the antibacterial activity.^{49,50} For Ti-AQ, the strong positive charge of QPEI was partially neutralized by negatively charged ALN, which showed lower cytotoxicity than that of Ti-Q. Moreover, conjugated ALN also has good compatibility for osteoblasts and high affinity for bone minerals.^{51–53} Therefore, Ti-AQ could support adhesion and proliferation of osteoblasts while possessing antibacterial abilities. According to the above results of in vitro antibacterial evaluation (Figure 2), Ti-A had no antibacterial effect and Ti-Q possessed strong cytotoxicity. Because of its good antibacterial and biocompatible performances, Ti-AQ was selected for an in vivo anti-infection and osteointegration study.

2.3. In Vivo Anti-Infection. To investigate the in vivo anti-infection ability of dual-functionalized implants, *S. aureus*-contaminated Ti-AQ samples were implanted into the distal femoral metaphysis of rats to simulate BAI in implantation (Figure S7, Supporting Information) because the micro-environment of cancellous bone in distal femoral metaphysis was similar to that in the alveolar bone. The pristine Ti implants used in the clinic were taken as controls. At 3 and 7 days after surgery, the femurs of experimental animals were harvested (Figure S8, Supporting Information). For evaluation of in vivo anti-infection, the implants in each group were isolated from the femurs and the bacteria on the surfaces of implants were rinsed by vortex and cultured on solid lysogeny broth media for 24 h (Figure 4a). The numbers of bacterial colonies of Ti-AQ were significantly lower than those of Ti

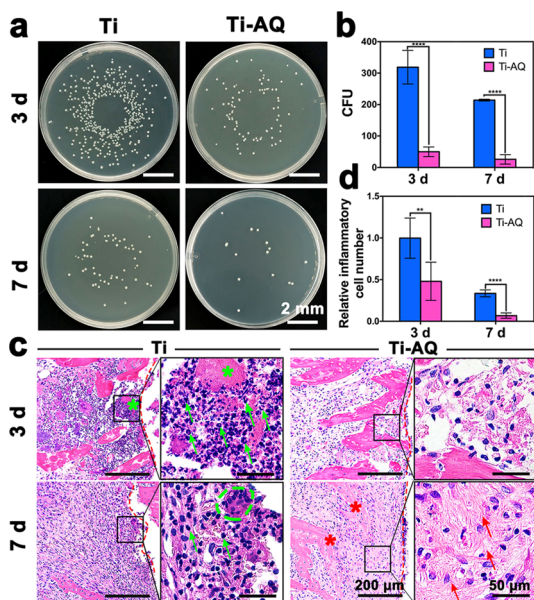


Figure 4. Representative images (a) and counting (b) of *S. aureus* colonies in the Ti and Ti-AQ groups after 3–7 days of implantation; (c) histological examination by hematoxylin–eosin (H&E) staining of the tissues around the implants of Ti and Ti-AQ; and (d) relative inflammatory cell numbers per unit area within the range of 500 μm from the implants. (Red dashed line, implant–tissue interfaces; green asterisks, necrotic tissue particles; green arrows, neutrophils; green dashed lines, multinuclear giant cells; red asterisks, immature trabecular; red arrows, fibrous connective tissue.) Statistical significance was determined using Student's *t*-test (**** $p < 0.0001$; *** $p < 0.001$; ** $p < 0.01$; data are represented as mean \pm s.d.).

(Figure 4b). These results demonstrated that the Ti-AQ implants could kill the bacteria adhered on the surfaces at the early stage of BAI.

Furthermore, the *in vivo* tissue inflammatory reaction was evaluated by histological analysis. The bone tissues around the implants were observed using hematoxylin–eosin (H&E) staining at 3 and 7 days after surgery (Figure 4c). At 3 days, obvious inflammation-associated cells (neutrophils, lymphocytes, etc.) were observed in the Ti group and they were mainly distributed in the necrotic tissue particles (green asterisks, Figure 4c), confirming the occurrence of bacterium-caused infection. Plenty of neutrophils (green arrows, Figure 4c) in the femoral medullary cavity and representative multinuclear giant cells with a huge cell body and multiple nuclei (green dashed circle, Figure 4c) were also found in the inflammatory tissues of the Ti group, indicating the acute inflammatory reaction and strong immune responses. On the other hand, due to the antibacterial properties of Ti-AQ, the infiltration of inflammatory cells was inhibited in the Ti-AQ group at 3 days (Figure 4c). At 7 days, the majority of the cells within the medullary cavity of Ti-AQ group were normal. Notably, immature trabecula (red asterisk, Figure 4c), one signal of new bone formation, were observed in the Ti-AQ group. On the contrary, residual inflammatory cells still could be found in the Ti group. To quantify the tissue inflammatory reaction, the inflammation-associated cell numbers per unit area were calculated (Figure 4d). The amounts of inflammatory cells in the Ti-AQ group were significantly lower than those of the Ti group. The histological results further confirmed that Ti-AQ had excellent *in vivo* antibacterial abilities. Therefore, by being functionalized with ALN and

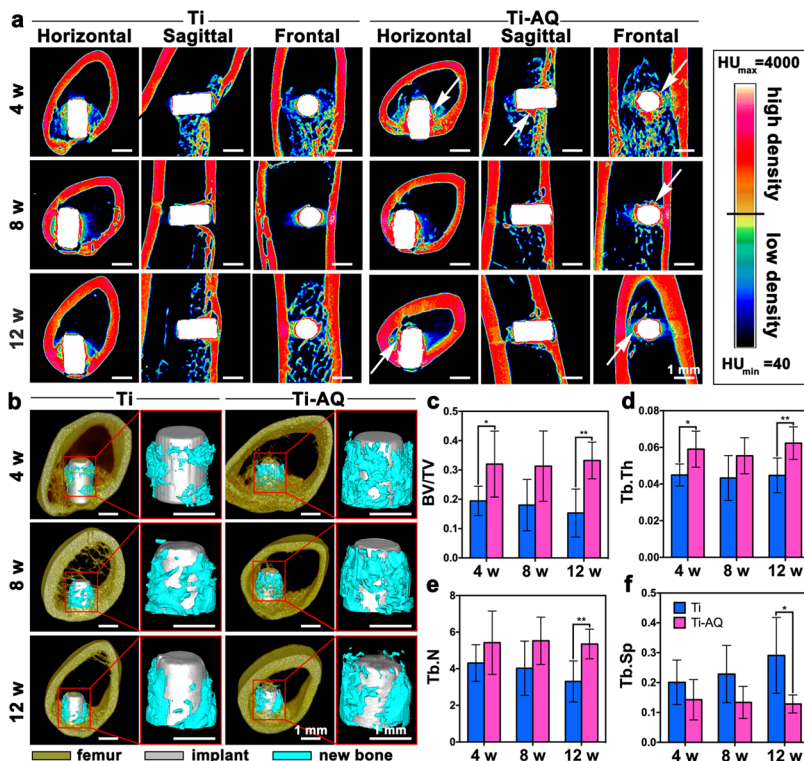


Figure 5. (a) Representative cross-sectional micro-CT images and density mapping (newly formed bone tissues were indicated by white arrows); (b) three-dimensional (3D) reconstruction of micro-CT scanning; (c) static histomorphometric analysis of bone volume/total volume (BV/TV), (d) Tb.Th, (e) Tb.N, and (f) Tb.Sp. Statistical significance was determined using Student's *t*-test (** $p < 0.01$; * $p < 0.05$; data are represented as mean \pm s.d.).

QPEI, the implants could possess satisfactory *in vivo* antibacterial properties and biocompatibility, which could suppress the inflammatory reaction in BAI models.

2.4. In Vivo Bone–Implant Osteointegration. Osteointegration is essential for the stability and retention of dental implants. To investigate the *in vivo* osteointegration-promoting ability of Ti-AQ under infected conditions, microcomputed tomography (micro-CT), dual-fluorochrome labeling, histological analysis, and biomechanical test were performed using BAI animal models from 4 to 12 weeks.

Micro-CT scanning of the femur samples with implants was first performed to evaluate the peri-implant new bone formation. The new bone formation was evaluated in the volume of interest (VOI) that was based on a peri-implant circle zone within 0.5 mm from the implant. The length of VOI started from the inner edge of cortical bone to the bottom of implant, which was divided into 80 slices (1.4 mm per slice in thickness, approximately). As shown in Figure 5a, no obvious new bone formation around the Ti implant was observed from cross-sectional (horizontal, sagittal, and frontal) views at 4 weeks. In contrast, new bone formation was found in the peri-implant area (white arrows, Figure 5a) of Ti-AQ at 4 weeks. These results demonstrated that Ti-AQ significantly enhanced new bone formation. After 12 weeks of surgery, the bone tissues in the Ti-AQ group continued forming over the Ti group, resulting in more new bone formation (white arrows, Figure 5a). Ti-AQ could improve new bone formation during the osteointegration process from the early stage (4 weeks after implantation) to the late stage (12 weeks after implantation) in the BAI animal models.

The peri-implant bone masses were also visualized using 3D reconstruction (Figure 5b). The bone masses around in the Ti-AQ implants were much larger than those in the Ti group at each time point. The peri-implant new bone formation was quantitatively analyzed by static histomorphometric indexes based on the results of micro-CT (Figure 5c–f). The bone volume/total volume (BV/TV) was the index of osteogenic capacity. The values of BV/TV for the Ti-AQ group were higher than those for the Ti group at each time point, indicating the better osteogenic capacity of the Ti-AQ implants in the BAI model. According to the above *in vivo* antibacterial results, QPEI could inhibit the peri-implant infection, which probably provided a suitable condition for new bone formation in the early stage of implantation. Along with the healing time, osteointegration between the native bones and implants was enhanced by the introduced ALN in the late stage. Similarly, the Ti-AQ group also showed better trabecular thickness (Tb.Th), trabecular number (Tb.N), and trabecular separation (Tb.Sp) values than those of the Ti group. These results demonstrated that dual functionalization of Ti-AQ could improve osteointegration of the implants. Numerous studies have demonstrated that the introduction of alendronate increased osteointegration by improving new bone formation, bone volume fraction, bone–material affinity, and biomechanical properties.^{54–57} More importantly, because ALN was covalently conjugated onto three-dimensional polymer brushes, ALN molecules would not be released from the surface. Therefore, osteonecrosis induced by free ALN could be avoided.^{23,43} Also, the high affinity of ALN with bone tissue was retained because the phosphate groups of ALN were not affected by conjugation, which was beneficial to the improvement of osteointegration.

To further investigate the osteointegration of bone–implant interfaces, the histomorphometric analysis was performed by undecalcified slicing of femur specimens with implants. The representative images of toluidine blue staining sections and double fluorochrome labeling sections are shown in Figure 6a.

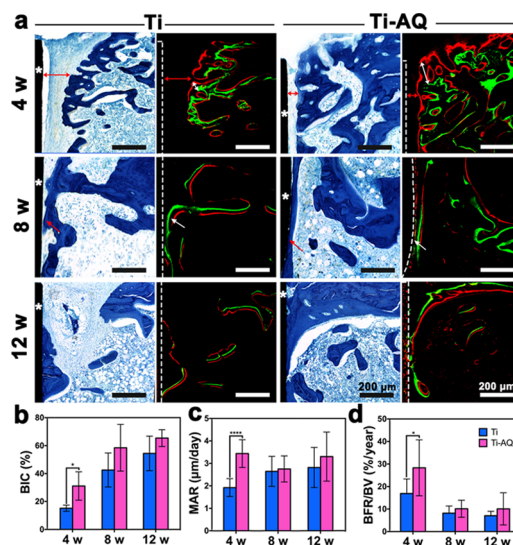


Figure 6. (a) Representative images of bone–implant interfaces by toluidine blue staining and calcein/alizarin red S double fluorescent labeling (white asterisks, implant; white dashed lines, the implant–bone interface; red double-headed asterisks, the gaps between implant and bone; red arrows and white arrows, newly formed bone tissues), (b) BIC percentage, (c) MAR values, and (d) BFR/BV values. Statistical significance was determined using Student's *t*-test (**** $p < 0.0001$; * $p < 0.05$; data are represented as mean \pm s.d.).

During the healing process from 4 to 12 weeks, no signs of inflammation or adverse tissue reactions were observed around the implants. The bone-to-implant contact (BIC), the most intuitive index for evaluating bone–implant osteointegration, was calculated based on the images of toluidine blue staining (Figure 6b). In addition, the bone matrix mineral apposition rate (MAR) and bone formation rate/BV (BFR/BV), important indexes of dynamic bone histomorphometry, were determined based on double fluorochrome labeling (Figure 6c,d). In the Ti-AQ group, immature bone trabecula were observed closed to the implant and the gaps between the trabecular bone and implant were smaller than those in the Ti group (red double-headed arrows in Figure 6a).

The percentage of BIC in the Ti-AQ group was nearly two times higher than that in Ti group at 4 weeks. From double fluorochrome labeling sections, the intervals between the red color lines (new bone deposition lines) and the green color lines (old bone deposition lines) were much larger than the Ti group at 4 weeks (white double-head arrows in Figure 6a). In the Ti-AQ group, the values of MAR and BFR/BV were significantly higher than those in the Ti group. These results further demonstrated that Ti-AQ implants promoted new bone formation at the early stage of bone–implant osteointegration, which was consistent with the results of 3D reconstruction images and static histomorphometric observation of micro-CT (Figure 5c–f). At 8 weeks, the results of the histological analysis showed more new bone formation in the area adjacent to the implant surfaces compared with those at 4 weeks in both groups. The high values of MAR and BFR/BV in the Ti-AQ

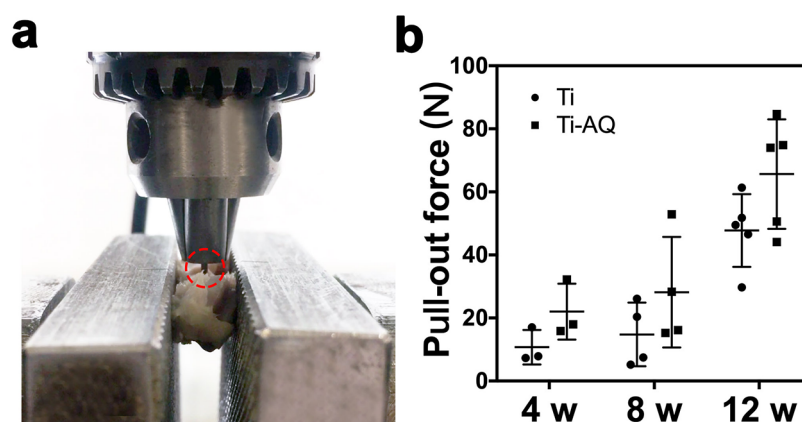


Figure 7. (a) Equipment of the pull-out test, where the implant clamped by the customized fixture was indicated by a red dashed circle, and (b) pull-out forces of the Ti and Ti-AQ groups at 4, 8, and 12 weeks.

group indicated the rapid rate of mineral deposition and new bone formation during the stage of bone–implant osteointegration.⁵⁸ Eventually, the bone tissues formed broad layers covering the surface of Ti-AQ at 12 weeks, demonstrating that the Ti-AQ implants could intensely improve the bone–implant osteointegration. Therefore, in the BAI animal model, the dual-functionalized Ti-AQ implants have played an essential role in improving the bone–implant osteointegration at the late stage, which enhanced the integration between the implant and bone tissue.

Furthermore, to evaluate the implantation stability, a biomechanical test was performed by the “pull-out” method (Figure 7a). The osteointegration was quantified by the maximum pull-out force of various groups of implants at 4, 8, and 12 weeks. The maximum pull-out forces of the Ti-AQ group were 26, 37, and 12% higher than those of the Ti group at 4, 8, and 12 weeks, respectively (Figure 7b). The results also demonstrated that Ti-AQ exhibited good stabilities in the BAI model, which will increase the long-term success ratio of dental implants under infected conditions.

3. CONCLUSIONS

In summary, dual-functional implants (Ti-AQ) with anti-bacterial and osteointegration-promoting properties were successfully constructed for the treatment of BAI. A cationic antibacterial agent, low-molecular-weight QPEI, and osteointegration-promoting component, ALN, were readily conjugated with polymer brushes via the Schiff base reaction. The in vitro studies proved that the Ti-AQ implant showed good antibacterial ability and favorable biocompatibility. The excellent in vivo anti-infection and osteointegration performances of Ti-AQ were demonstrated using a BAI animal model. When the implants were contaminated by bacteria, the Ti-AQ implant could prevent the infection at the early stage, which developed a supportive environment for bone–implant osteointegration during the following long-term healing period, leading to the high biomechanical stability of implants. The present work provided a promising strategy for the design and development of novel multifunctional implants.

4. EXPERIMENTAL SECTION

The detailed experimental methods were described in the [Supporting Information](#).

■ ASSOCIATED CONTENT

📄 Supporting Information

The Supporting Information is available free of charge on the [ACS Publications website](#) at DOI: [10.1021/acsami.9b14572](https://doi.org/10.1021/acsami.9b14572).

Experimental methods; scheme of the dual-functionalization process; ¹H NMR spectrum of QPEI; cross-sectional image of Ti-GA; water contact angles; ATR-FTIR spectra; XPS spectra; surface element ratios; and in vivo experimental process and general views of the femur samples with implants ([PDF](#))

■ AUTHOR INFORMATION

Corresponding Authors

*E-mail: duanshun@mail.buct.edu.cn (S.D.).

*E-mail: zhihui_tang@126.com (Z.T.).

*E-mail: xufj@mail.buct.edu.cn (F.-J.X.).

ORCID

Fu-Jian Xu: [0000-0002-1838-8811](https://orcid.org/0000-0002-1838-8811)

Notes

The authors declare no competing financial interest.

[§]Y.S. and Y.-Q.Z. contributed equally to this work.

■ ACKNOWLEDGMENTS

This work was supported by the National Key Research and Development Program of China (Grant nos. 2016YFC1100404 and 2016YFB1101200), National Natural Science Foundation of China (Grant nos. 51873012 and 51733001), Beijing Municipal Natural Science Foundation (Grant no. 7161001), Fundamental Research Funds for the Central Universities (Grant no. XK1802-2), and Research Projects on Biomedical Transformation of China-Japan Friendship Hospital (Grant no. PYBZ1832).

■ REFERENCES

- Roy-Chaudhury, P.; Munda, R. Infections Associated with Surgical Implants. *N. Engl. J. Med.* **2004**, *351*, 193–194.
- Del Pozo, J. L.; Patel, R. Infection Associated with Prosthetic Joints. *N. Engl. J. Med.* **2009**, *361*, 787–794.
- Kapadia, B. H.; Berg, R. A.; Daley, J. A.; Fritz, J.; Bhave, A.; Mont, M. A. Periprosthetic Joint Infection. *Lancet* **2016**, *387*, 386–394.
- Darouiche, R. O. Treatment of Infections Associated with Surgical Implants. *N. Engl. J. Med.* **2004**, *350*, 1422–1426.

- (5) Ferguson, R. J.; Palmer, A. J. R.; Taylor, A.; Porter, M. L.; Malchau, H.; Glyn-Jones, S. Hip Replacement. *Lancet* **2018**, *392*, 1662–1671.
- (6) Bauer, S.; Schmuki, P.; von der Mark, K.; Park, J. Engineering Biocompatible Implant Surfaces. *Prog. Mater. Sci.* **2013**, *58*, 261–326.
- (7) Persson, G. R.; Renvert, S. Cluster of Bacteria Associated with Peri-Implantitis. *Clin. Implant Dent. Relat. Res.* **2014**, *16*, 783–793.
- (8) O'Connor, A. M.; McManus, B. A.; Kinnevey, P. M.; Brennan, G. I.; Fleming, T. E.; Cashin, P. J.; O'Sullivan, M.; Palyzois, L.; Coleman, D. C. Significant Enrichment and Diversity of the Staphylococcal Arginine Catabolic Mobile Element ACME in *Staphylococcus epidermidis* Isolates from Subgingival Peri-Implantitis Sites and Periodontal Pockets. *Front. Microbiol.* **2018**, *9*, No. 1558.
- (9) Arciola, C. R.; Campoccia, D.; Montanaro, L. Implant Infections: Adhesion, Biofilm Formation and Immune Evasion. *Nat. Rev. Microbiol.* **2018**, *16*, 397–409.
- (10) Wei, T.; Yu, Q.; Chen, H. Responsive and Synergistic Antibacterial Coatings: Fighting Against Bacteria in a Smart and Effective Way. *Adv. Healthcare Mater.* **2019**, *8*, No. 1801381.
- (11) Liu, W.; Li, J.; Cheng, M.; Wang, Q.; Qian, Y.; Yeung, K. W. K.; Chu, P. K.; Zhang, X. A Surface-Engineered Polyetheretherketone Biomaterial Implant with Direct and Immunoregulatory Antibacterial Activity against Methicillin-Resistant *Staphylococcus aureus*. *Biomaterials* **2019**, *208*, 8–20.
- (12) Spriano, S.; Yamaguchi, S.; Bains, F.; Ferraris, S. A Critical Review of Multifunctional Titanium Surfaces: New Frontiers for Improving Osseointegration and Host Response, Avoiding Bacteria Contamination. *Acta Biomater.* **2018**, *79*, 1–22.
- (13) Tobin, E. J. Recent Coating Developments for Combination Devices in Orthopedic and Dental Applications: A Literature Review. *Adv. Drug Delivery Rev.* **2017**, *112*, 88–100.
- (14) Li, X.; Wu, B.; Chen, H.; Nan, K.; Jin, Y.; Sun, L.; Wang, B. Recent Developments in Smart Antibacterial Surfaces to Inhibit Biofilm Formation and Bacterial Infections. *J. Mater. Chem. B* **2018**, *6*, 4274–4292.
- (15) Zhu, Y.; Xu, C.; Zhang, N.; Ding, X.; Yu, B.; Xu, F. J. Polycationic Synergistic Antibacterial Agents with Multiple Functional Components for Efficient Anti-Infective Therapy. *Adv. Funct. Mater.* **2018**, *28*, No. 1706709.
- (16) Zeng, Q.; Zhu, Y.; Yu, B.; Sun, Y.; Ding, X.; Xu, C.; Wu, Y. W.; Tang, Z.; Xu, F. J. Antimicrobial and Antifouling Polymeric Agents for Surface Functionalization of Medical Implants. *Biomacromolecules* **2018**, *19*, 2805–2811.
- (17) Pan, C.; Zhou, Z.; Yu, X. Coatings as the Useful Drug Delivery System for the Prevention of Implant-Related Infections. *J. Orthop. Surg. Res.* **2018**, *13*, No. 220.
- (18) Mei, S.; Wang, H.; Wang, W.; Tong, L.; Pan, H.; Ruan, C.; Ma, Q.; Liu, M.; Yang, H.; Zhang, L.; Cheng, Y.; Zhang, Y.; Zhao, L.; Chu, P. K. Antibacterial Effects and Biocompatibility of Titanium Surfaces with graded silver incorporation in Titania Nanotubes. *Biomaterials* **2014**, *35*, 4255–4265.
- (19) Bakhshandeh, S.; Amin Yavari, S. Electrophoretic Deposition: A Versatile Tool against Biomaterial Associated Infections. *J. Mater. Chem. B* **2018**, *6*, 1128–1148.
- (20) Xu, L. Q.; Neoh, K. G.; Kang, E. T. Natural Polyphenols as Versatile Platforms for Material Engineering and Surface Functionalization. *Prog. Polym. Sci.* **2018**, *87*, 165–196.
- (21) Tan, L.; Li, J.; Liu, X.; Cui, Z.; Yang, X.; Zhu, S.; Li, Z.; Yuan, X.; Zheng, Y.; Yeung, K. W. K.; Pan, H.; Wang, X.; Wu, S. Rapid Biofilm Eradication on Bone Implants Using Red Phosphorus and Near-Infrared Light. *Adv. Mater.* **2018**, *30*, No. 1801808.
- (22) Tan, L.; Li, J.; Liu, X. M.; Cui, Z. D.; Yang, X. J.; Yeung, K. W. K.; Pan, H.; Zheng, Y. F.; Wang, X. B.; Wu, S. In Situ Disinfection through Photoinspired Radical Oxygen Species Storage and Thermal-Triggered Release from Black Phosphorus with Strengthened Chemical Stability. *Small* **2018**, *14*, No. 1703197.
- (23) Zoppe, J. O.; Ataman, N. C.; Mocny, P.; Wang, J.; Moraes, J.; Klok, H. A. Surface-Initiated Controlled Radical Polymerization: State-of-the-Art, Opportunities, and Challenges in Surface and Interface Engineering with Polymer Brushes. *Chem. Rev.* **2017**, *117*, 1105–1318.
- (24) Qian, Y.; Qi, F.; Chen, Q.; Zhang, Q.; Qiao, Z.; Zhang, S.; Wei, T.; Yu, Q.; Yu, S.; Mao, Z.; Gao, C.; Ding, Y.; Cheng, Y.; Jin, C.; Xie, H.; Liu, R. Surface Modified with a Host Defense Peptide-Mimicking Beta-Peptide Polymer Kills Bacteria on Contact with High Efficacy. *ACS Appl. Mater. Interfaces* **2018**, *10*, 15395–15400.
- (25) Jin, X.; Xiong, Y. H.; Zhang, X. Y.; Wang, R.; Xing, Y.; Duan, S.; Chen, D.; Tian, W.; Xu, F. J. Self-Adaptive Antibacterial Porous Implants with Sustainable Responses for Infected Bone Defect Therapy. *Adv. Funct. Mater.* **2019**, *29*, No. 1807915.
- (26) Yuan, H.; Yu, B.; Fan, L. H.; Wang, M.; Zhu, Y.; Ding, X.; Xu, F. J. Multiple Types of Hydroxyl-Rich Cationic Derivatives of PGMA for Broad-Spectrum Antibacterial and Antifouling Coatings. *Polym. Chem.* **2016**, *7*, 5709–5718.
- (27) Matyjaszewski, K. Advanced Materials by Atom Transfer Radical Polymerization. *Adv. Mater.* **2018**, *30*, No. 1706441.
- (28) Chen, T.; Yang, H.; Wu, X.; Yu, D.; Ma, A.; He, X.; Sun, K.; Wang, J. Ultrahighly Charged Amphiphilic Polymer Brushes with Super-Antibacterial and Self-Cleaning Capabilities. *Langmuir* **2019**, *35*, 3031–3037.
- (29) Valencia, L.; Kumar, S.; Jalvo, B.; Mautner, A.; Salazar-Alvarez, G.; Mathew, A. P. Fully Bio-Based Zwitterionic Membranes with Superior Antifouling and Antibacterial Properties Prepared via Surface-Initiated Free-Radical Polymerization of Poly(Cysteine Methacrylate). *J. Mater. Chem. A* **2018**, *6*, 16361–16370.
- (30) Muszanska, A.; Busscher, H. J.; Herrmann, A.; van der Mei, H. C.; Norde, W. Pluronic–Lysozyme Conjugates as Anti-Adhesive and Antibacterial Bifunctional Polymers for Surface Coating. *Biomaterials* **2011**, *32*, 6333–6341.
- (31) Wang, X.; Yan, S.; Song, L.; Shi, H.; Yang, H.; Luan, S.; Huang, Y.; Yin, J.; Khan, A. F.; Zhao, J. Temperature-Responsive Hierarchical Polymer Brushes Switching from Bactericidal to Cell Repellency. *ACS Appl. Mater. Interfaces* **2017**, *9*, 40930–40939.
- (32) Yan, S.; Shi, H.; Song, L.; Wang, X.; Liu, L.; Luan, S.; Yang, Y.; Yin, J. Nonleaching Bacteria-Responsive Antibacterial Surface Based on a Unique Hierarchical Architecture. *ACS Appl. Mater. Interfaces* **2016**, *8*, 24471–24481.
- (33) Ding, X.; Duan, S.; Ding, X.; Liu, R.; Xu, F. J. Versatile Antibacterial Materials: An Emerging Arsenal for Combatting Bacterial Pathogens. *Adv. Funct. Mater.* **2018**, *28*, No. 1802140.
- (34) Hoyos-Nogués, M.; Velasco, F.; Ginebra, M. P.; Manero, J. M.; Gil, F. J.; Mas-Moruno, C. Regenerating Bone via Multifunctional Coatings: The Blending of Cell Integration and Bacterial Inhibition Properties on the Surface of Biomaterials. *ACS Appl. Mater. Interfaces* **2017**, *9*, 21618–21630.
- (35) Devlin-Mullin, A.; Todd, N. M.; Golrokhi, Z.; Geng, H.; Knerding, M. A.; Ternan, N. G.; Hunt, J. A.; Potter, R. J.; Sutcliffe, C.; Jones, E.; Lee, P. D.; Mitchell, C. A. Atomic Layer Deposition of a Silver Nanolayer on Advanced Titanium Orthopedic Implants Inhibits Bacterial Colonization and Supports Vascularized De Novo Bone Ingrowth. *Adv. Healthcare Mater.* **2017**, *6*, No. 1700033.
- (36) Cheng, H.; Yue, K.; Kazemzadeh-Narbat, M.; Liu, Y.; Khalilpour, A.; Li, B.; Zhang, Y. S.; Annabi, N.; Khademhosseini, A. Mussel-Inspired Multifunctional Hydrogel Coating for Prevention of Infections and Enhanced Osteogenesis. *ACS Appl. Mater. Interfaces* **2017**, *9*, 11428–11439.
- (37) Jiang, H.; Xu, F. J. Biomolecule-Functionalized Polymer Brushes. *Chem. Soc. Rev.* **2013**, *42*, 3394–3426.
- (38) Xu, F. J.; Wang, Z. H.; Yang, W. T. Surface Functionalization of Polycaprolactone Films via Surface-Initiated Atom Transfer Radical Polymerization for Covalently Coupling Cell-Adhesive Biomolecules. *Biomaterials* **2010**, *31*, 3139–3147.
- (39) Harrison, R. H.; Steele, J. A.; Chapman, R.; Gormley, A. J.; Chow, L. W.; Mahat, M. M.; Podhorska, L.; Palgrave, R. G.; Payne, D. J.; Hettiaratchy, S. P.; Dunlop, I. E.; Stevens, M. M. Modular and Versatile Spatial Functionalization of Tissue Engineering Scaffolds through Fiber-Initiated Controlled Radical Polymerization. *Adv. Funct. Mater.* **2015**, *25*, 5748–5757.

- (40) Guo, W.; Xiong, L.; Reese, C. M.; Amato, D. V.; Thompson, B. J.; Logan, P. K.; Patton, D. L. Post-Polymerization Modification of Styrene–Maleic Anhydride Copolymer Brushes. *Polym. Chem.* **2017**, *8*, 6778–6785.
- (41) Mas-Moruno, C.; Su, B.; Dalby, M. J. Multifunctional Coatings and Nanotopographies: Toward Cell Instructive and Antibacterial Implants. *Adv. Healthcare Mater.* **2019**, *8*, No. 1801103.
- (42) Li, J.; Tan, L.; Liu, X. M.; Cui, Z. D.; Yang, X. J.; Yeung, K. W. K.; Chu, P. K.; Wu, S. Balancing Bacteria-Osteoblast Competition through Selective Physical Puncture and Biofunctionalization of ZnO/Polydopamine/Arginine-Glycine-Aspartic Acid-Cysteine Nanorods. *ACS Nano* **2017**, *11*, 11250–11263.
- (43) McClung, M.; Harris, S. T.; Miller, P. D.; Bauer, D. C.; Davison, K. S.; Dian, L.; Hanley, D. A.; Kendler, D. L.; Yuen, C. K.; Lewiecki, E. M. Bisphosphonate Therapy for Osteoporosis: Benefits, Risks, and Drug Holiday. *Am. J. Med.* **2013**, *126*, 13–20.
- (44) Ryu, J. H.; Messersmith, P. B.; Lee, H. Polydopamine Surface Chemistry: A Decade of Discovery. *ACS Appl. Mater. Interfaces* **2018**, *10*, 7523–7540.
- (45) Tiller, J. C.; Liao, C. J.; Lewis, K.; Klivanov, A. M. Designing Surfaces That Kill Bacteria on Contact. *Proc. Natl. Acad. Sci. U.S.A.* **2001**, *98*, 5981–5985.
- (46) Liu, X.; Wang, S. Three-Dimensional Nano-Biointerface as a New Platform for Guiding Cell Fate. *Chem. Soc. Rev.* **2014**, *43*, 2385–2401.
- (47) Zehra, N.; Dutta, D.; Malik, A. H.; Ghosh, S. S.; Iyer, P. K. Fluorescence Resonance Energy Transfer-Based Wash-Free Bacterial Imaging and Antibacterial Application Using a Cationic Conjugated Polyelectrolyte. *ACS Appl. Mater. Interfaces* **2018**, *10*, 27603–27611.
- (48) Sun, H.; Hong, Y.; Xi, Y.; Zou, Y.; Gao, J.; Du, J. Synthesis, Self-Assembly, and Biomedical Applications of Antimicrobial Peptide-Polymer Conjugates. *Biomacromolecules* **2018**, *19*, 1701–1720.
- (49) Tejero, R.; Gutierrez, B.; Lopez, D.; Lopez-Fabal, F.; Gomez-Garcés, J. L.; Fernandez-Garcia, M. Copolymers of Acrylonitrile with Quaternizable Thiazole and Triazole Side-Chain Methacrylates as Potent Antimicrobial and Hemocompatible Systems. *Acta Biomater.* **2015**, *25*, 86–96.
- (50) Fan, X. L.; Hu, M.; Qin, Z. H.; Wang, J.; Chen, X. C.; Lei, W. X.; Ye, W. Y.; Jin, Q.; Ren, K. F.; Ji, J. Bactericidal and Hemocompatible Coating via the Mixed-Charged Copolymer. *ACS Appl. Mater. Interfaces* **2018**, *10*, 10428–10436.
- (51) Chen, Q.; Zheng, C.; Li, Y.; Bian, S.; Pan, H.; Zhao, X.; Lu, W. W. Bone Targeted Delivery of SDF-1 via Alendronate Functionalized Nanoparticles in Guiding Stem Cell Migration. *ACS Appl. Mater. Interfaces* **2018**, *10*, 23700–23710.
- (52) Forte, L.; Torricelli, P.; Boanini, E.; Gazzano, M.; Fini, M.; Bigi, A. Antiresorptive and Anti-Angiogenetic Octacalcium Phosphate Functionalized with Bisphosphonates: An In Vitro Tri-Culture Study. *Acta Biomater.* **2017**, *54*, 419–428.
- (53) Zheng, D.; Neoh, K. G.; Kang, E. T. Immobilization of Alendronate on Titanium via Its Different Functional Groups and the Subsequent Effects on Cell Functions. *J. Colloid Interface Sci.* **2017**, *487*, 1–11.
- (54) Bobyn, J. D.; Thompson, R.; Lim, L.; Pura, J. A.; Bobyn, K.; Tanzer, M. Local Alendronate Acid Elution Increases Net Periimplant Bone Formation: A Micro-CT Analysis. *Clin. Orthop. Relat. Res.* **2014**, *472*, 687–694.
- (55) Salamanna, F.; Giavaresi, G.; Parrilli, A.; Torricelli, P.; Boanini, E.; Bigi, A.; Fini, M. Antiresorptive Properties of Strontium Substituted and Alendronate Functionalized Hydroxyapatite Nanocrystals in an Ovariectomized Rat Spinal Arthrodesis Model. *Mater. Sci. Eng. C* **2019**, *95*, 355–362.
- (56) Wang, Y.; Huang, Q.; He, X.; Chen, H.; Zou, Y.; Li, Y.; Lin, K.; Cai, X.; Xiao, J.; Zhang, Q.; Cheng, Y. Multifunctional Melanin-Like Nanoparticles for Bone-Targeted Chemo-Photothermal Therapy of Malignant Bone Tumors and Osteolysis. *Biomaterials* **2018**, *183*, 10–19.
- (57) Cotts, K. G.; Cifu, A. S. Treatment of Osteoporosis. *JAMA* **2018**, *319*, 1040–1041.
- (58) Parfitt, A. M.; Drezner, M. K.; Glorieux, F. H.; Kanis, J. A.; Malluche, H.; Meunier, P. J.; Ott, S. M.; Recker, R. R. Bone Histomorphometry: Standardization of Nomenclature, Symbols, and Units. Report of the ASBMR Histomorphometry Nomenclature Committee. *J. Bone Miner. Res.* **1987**, *2*, 595–610.